The Journal of Physical Chemistry Letters

Subscriber access provided by SDIS @ INRS | http://sdis.inrs.ca

Physical Insights into Chemistry, Catalysis, and Interfaces

Alkamides and Piperamides as Potential Antivirals Against the Severe Acute Respiratory Syndrome Coronavirus 2 (SARS-CoV-2)

Juan Manuel Gutierrez-Villagomez, Tonatiu Campos-García, Jorge Molina Torres, Mercedes G. López, and Juan Vázquez-Martínez

J. Phys. Chem. Lett., **Just Accepted Manuscript** • DOI: 10.1021/acs.jpclett.0c01685 • Publication Date (Web): 25 Aug 2020

Downloaded from pubs.acs.org on September 1, 2020

Just Accepted

"Just Accepted" manuscripts have been peer-reviewed and accepted for publication. They are posted online prior to technical editing, formatting for publication and author proofing. The American Chemical Society provides "Just Accepted" as a service to the research community to expedite the dissemination of scientific material as soon as possible after acceptance. "Just Accepted" manuscripts appear in full in PDF format accompanied by an HTML abstract. "Just Accepted" manuscripts have been fully peer reviewed, but should not be considered the official version of record. They are citable by the Digital Object Identifier (DOI®). "Just Accepted" is an optional service offered to authors. Therefore, the "Just Accepted" Web site may not include all articles that will be published in the journal. After a manuscript is technically edited and formatted, it will be removed from the "Just Accepted" Web site and published as an ASAP article. Note that technical editing may introduce minor changes to the manuscript text and/or graphics which could affect content, and all legal disclaimers and ethical guidelines that apply to the journal pertain. ACS cannot be held responsible for errors or consequences arising from the use of information contained in these "Just Accepted" manuscripts.

is published by the American Chemical Society. 1155 Sixteenth Street N.W., Washington, DC 20036

Published by American Chemical Society. Copyright © American Chemical Society. However, no copyright claim is made to original U.S. Government works, or works produced by employees of any Commonwealth realm Crown government in the course of their duties.

Alkamides and Piperamides as Potential Antivirals Against the Severe Acute Respiratory Syndrome Coronavirus 2 (SARS-CoV-2)

*Juan Manuel Gutierrez-Villagomez†, Tonatiu Campos-García‡, Jorge Molina-Torres‡, Mercedes G. López‡, Juan Vázquez-Martínez**

† Institut National de la Recherche Scientifique (INRS), Centre Eau Terre Environnement, Québec, Quebec, G1K 9A9, Canada.

‡ Departamento de Biotecnología y Bioquímica, Centro de Investigación y de Estudios Avanzados del IPN (CINVESTAV) Unidad Irapuato, 36824, Irapuato, Guanajuato, Mexico.

* Instituto Tecnológico Superior de Irapuato, TecNM, 36821, Irapuato, Guanajuato, Mexico

AUTHOR INFORMATION

Corresponding Author

* Juan Vázquez-Martínez – Instituto Tecnológico Superior de Irapuato, TecNM, 36821, Irapuato, Guanajuato, Mexico; orcid.org/0000-0002-3037-1457;

E-mail: juan.vazquez@itesi.edu.mx; juan.vm@irapuato.tecnm.mx

ABSTRACT. The pandemic caused by the SARS-CoV-2 has quickly spread globally, infecting millions, and killing hundreds of thousands of people. Herein, to identify potential antiviral agents, 97 natural amide-like compounds known as alkamides and piperamides were tested against SARS-CoV-2 main protease (Mpro) and RNA-dependent RNA polymerase (RdRp), and the human angiotensin-converting enzyme 2 (ACE2) using molecular docking and molecular dynamics simulations. The docking results showed that alkamides and dimeric piperamides from *Piper* species have a high binding affinity and potential antiviral activity against SARS-CoV-2. The absorption, distribution, metabolism and excretion (ADME) profile and Lipinski's rule of five showed that dimeric piperamides have druglikeness potential. The molecular dynamics results showed that pipercyclobutanamide B forms a complex with Mpro

at a similar level of stability than N3-I. Our overall results indicate that alkamides and piperamides, and specifically pipercyclobutanamide B should be further studied as compounds with SARS-CoV-2 antiviral properties.

TOC GRAPHICS

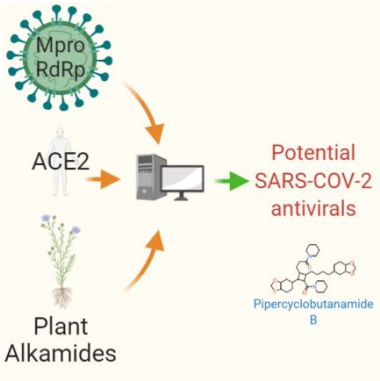

KEYWORDS. COVID-19; Mpro; RdRp; ACE2; *in silico* analysis; capsaicinoids.

Coronaviruses are a type of single-stranded positive-sense RNA viruses ((+)ssRNA) and are classified in four groups: alfa, beta, delta, and gamma coronaviruses.[1] Three new beta coronaviruses have been identified in the last two decades: the severe acute respiratory syndrome (SARS-CoV) in 2003,[2] the Middle

East respiratory syndrome coronavirus (MERS-CoV) in 2012,[3] and the severe acute respiratory syndrome coronavirus 2 (SARS-CoV-2) in 2019.[4] SARS-CoV-2 rapidly propagated and was declared a pandemic by the World Health Organization (WHO). MERS-CoV and SARS-CoV induce a mortality rate of 35 and 10% in humans, respectively.[5] The mortality rate by SARS-CoV-2 in humans ranges from 2 to 10%, depending on the country.[6,7] Coronavirus disease (COVID-19) is the infectious disease caused by SARS-CoV-2 and around 1/5 of infected people become seriously ill and present difficult breathing. People with diabetes, heart diseases, high blood pressure and cancer, as well as older people are considered high risk.[8]

The SARS-CoV and MERS-CoV outbreaks were contained and the development of vaccines or antiviral drugs for coronaviruses was relegated.[5] As of August 11th, 2020, there are more than 20 M confirmed COVID cases and more than 738 K deaths worldwide.[6] With the magnitude of the pandemic and its consequences, there is a dire need for treatments. Some research groups are focusing on developing vaccines and repurposing approved antivirals, while others are searching for novel antivirals.[9] A target for these antivirals is the non-structural main coronavirus

protease 3-chymotrypsin-like-protease (3CLpro, Nsp5 or Mpro), which is essential for the maturation of proteins during the viral cycle.[5,10–13] Other viral proteins marked as targets include the RNA-dependent RNA polymerase (RdRp, Nsp12), crucial for the SARS-CoV-2 life cycle,[14,15] and the angiotensin-converting enzyme 2 (ACE2), a human integral membrane glycoprotein highly expressed in the kidneys, heart, and pulmonary endothelium.[16,17] SARS-CoV-2 and other coronaviruses use ACE2 as a cellular entry receptor, specifically, the union of the spike protein S1 of SARS-CoV-2 to the enzymatic domain of ACE2 in the extracellular surface induces endocytosis and translocation of the virus-ACE2 protein complex.[18,19] Therefore, inhibiting the active sites of Mpro, RdRp and/or ACE2 is a potential approach for antiviral development.

Compounds containing amide and aromatic groups, including the approved COVID-19 drug Remdesivir, are potential inhibitors of Mpro, RdRp and/or ACE2.[5,10,11,15,20] In this regard, we evaluated the possible antiviral activity of natural, plant-derived, amide-like compounds known as alkamides and piperamides. Alkamides and piperamides are compounds structurally diverse comprised of

aromatic, polysubstituted, polyunsaturated and dimeric compounds, generally synthesized from the enzymatic reaction between acyl chains and amino acid-derived compounds.[21–23] These compounds have shown bioactivity in viruses, bacteria, fungi, and animals including humans.[22,24–27] Thus, we explored the interaction between 97 alkamides and piperamides and Mpro, RdRp and ACE2 using molecular docking simulations. Additionally, we study the interaction of the best-docked compound against Mpro using molecular dynamics (MD) simulations.

The docking score energy values (DS) generated from the binding of the processed-6LU7 structure and the compounds with the best DS are listed in Table 1 (See Table S1). The compounds with at least 70% of the N3-I (Mpro native inhibitor) DS values were considered as potential Mpro inhibitors. The best-docked compound against SARS-CoV-2 Mpro was pipercyclobutanamide B (DS = -7.827 Kcal/mol) which is comparable to N3-I (DS = -7.348 Kcal/mol). Others with considerable DS were *N*-(2-phenylethyl)-3-phenyl-2*E*-propenamide (DS = -5.963 Kcal/mol), pipercyclobutanamide A (DS = -7.244 Kcal/mol), nigramide R (DS = -6.979 Kcal/mol), nigramide Q (DS = -5.968 Kcal/mol), chabamide K (DS = -6.381

Kcal/mol), chabamide J (DS = -5.713 Kcal/mol) and chabamide I (DS = -5.346 Kcal/mol). Figure 1 and Table 2 show the molecular interactions of N3-I and pipercyclobutanamide B with Mpro. N3-I fits into the pocket of the active site of Mpro (Figures 1B-C). As well, pipercyclobutanamide B fits into the Mpro pocket (Figures 1E-F), but on the opposite side of N3-I (Figures 1B-C). The N3-I binding is mainly via polar interactions whereas pipercyclobutanamide B binds mainly through hydrophobic ones. Polar interactions are influenced mainly by amino and carbonyl groups (Figure 1A). The hydrophobic interactions are influenced mainly by aromatic rings and double bonds (Figure 1D).

Table 1. Docking scores, chemical species, and plant distribution of selected alkamides and piperamides docked against SARS-CoV-2 Mpro and RdRp, and to human ACE2 protein.

Number	Plant Genus	Alkamide/Piperamide type	Compound name	Chemical structure	MW (g/mol	Docking score (Kcal/mol) against

		Amine moiety	Acyl moiety			)	Mpro	RdRp	ACE2
2	*Acmella*	IB	PLN	*N*-isobutyl-(2*E*,4*Z*)-octadienamide	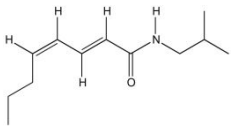	195.3	-4.592	-2.94	-4.385
4	*Acmella*	PHE	Other	*N*-(2-phenylethyl)-3-phenyl-2*E*-propenamide	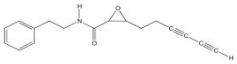	251.3	-5.963	-3.946	-5.882
5	*Acmella*	PHE	Other	*N*-(2-phenylethyl)-*cis*-2,3-epoxynona-6,8-diynamide	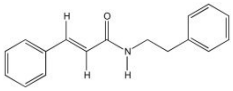	267.3	-3.943	-1.46	-1.925
43	*Nicotiana*	Cinnamoylphenethyl		Feruloyltyramine	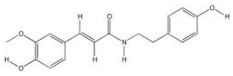	313,3	*	-4.814	*
48	*Piper*	Dimeric Piperamide		Chabamide I	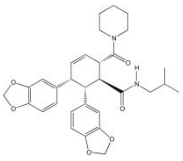	532.6	-5.346	-3.919	-4.36

49	*Piper*	Dimeric Piperamide	Chabamide J	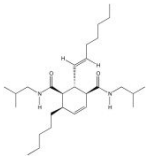	446.7	-5.713	-3.094	-3.683
50	*Piper*	Dimeric Piperamide	Chabamide K	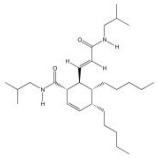	446.7	-6.381	-3.242	-3.926
56	*Piper*	Dimeric Piperamide	Nigramide Q	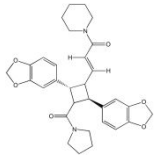	544.6	-5.968	-4.359	-6.855
57	*Piper*	Dimeric Piperamide	Nigramide R	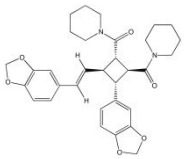	544.6	-6.979	-3.884	-6.585
58	*Piper*	Dimeric Piperamide	Pipercyclobutanamide A	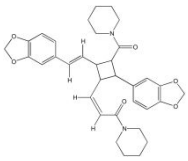	570.7	-7.244	-5.417	-6.997
59	*Piper*	Dimeric Piperamide	Pipercyclobutanamide B	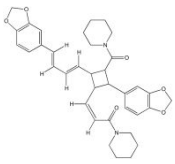	596.7	-7.827	-4.019	-7.34
62	*Piper*	Piperamide	8,9-Dihydropiplartine	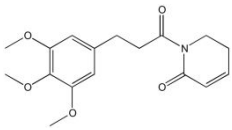	319.4	*	-5.432	*
64	*Piper*	Piperamide	*cis*-Piplartine	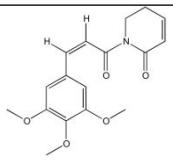	317.3	*	-5.073	*
	Native protein inhibitors							

98	N3-I (*N*-[(5-Methyl-1,2-oxazol-3-yl)carbonyl]-L-alanyl-L-valyl-*N*-{(2*S*,3*E*)-5-(benzyloxy)-5-oxo-1-[(3*S*)-2-oxo-3-pyrrolidinyl]-3-penten-2-yl}-L-leucinamide) Mpro Inhibitor	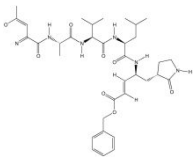	680.8	-7.348	#	#
99	GS-441524-TPP ((2*R*,3*R*,4*S*,5*R*)-2-(4-Aminopyrrolo[2,1-f][1,2,4]triazin-7-yl)-3,4-dihydroxy-5-(hydroxymethyl)oxolane-2-carbonitrile-TPP) RdRp polymerase Inhibitor	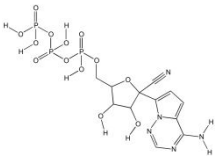	531.2	#	-8.495	#
100	DCBICA ((*S*,*S*)-2-{1-Carboxy-2-[3-(3,5-dichloro-benzyl)-3H-imidazol-4-YL]-ethylamino}-4-methyl-pentanoic acid) Human ACE2 protein Inhibitor	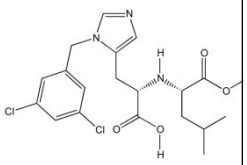	428.3	#	#	-10.56

Amine moiety: IB = Isobutyl, MB = 2-Methylbutyl, PHE = Phenylethyl. Acyl moiety: ACT = Acetylenic, PLN = Polyunsaturated, NST = Monounsaturated. * = Not docked. # = Not tested. TPP = Triphosphate.

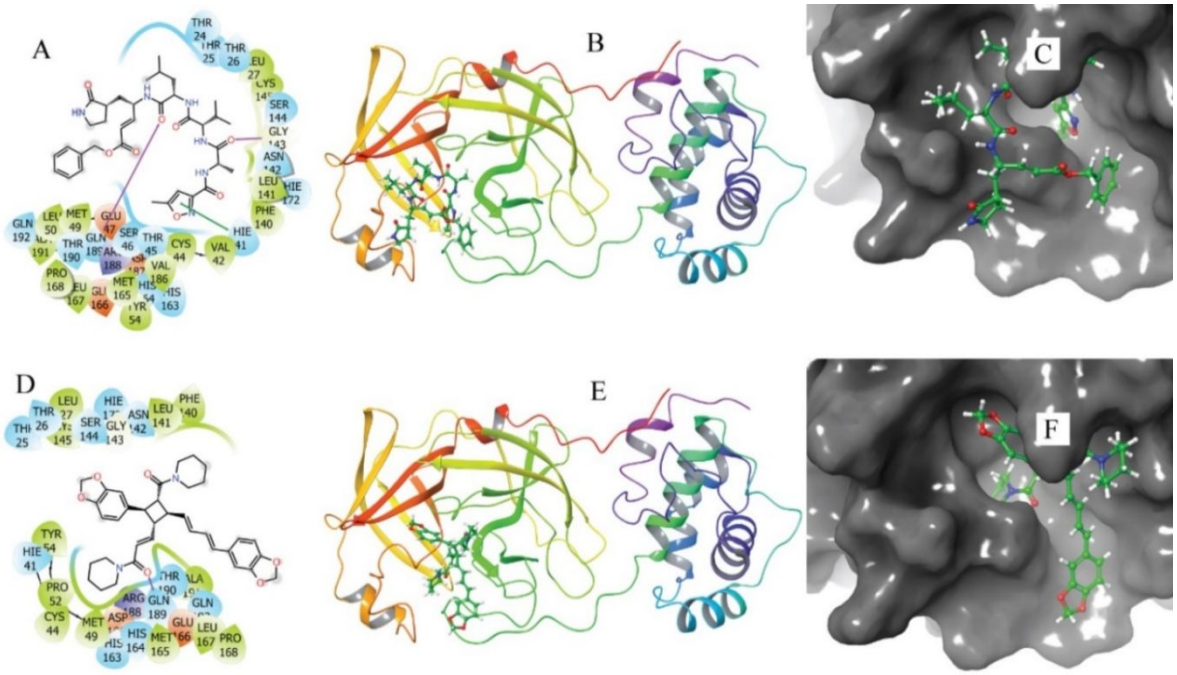

Figure 1. Molecular docking for SARS-CoV-2 Mpro against N3-I (A, B, C) and pipercyclobutanamide B (D, E, F). Interaction representations of the complexes N3-I-Mpro (A) and pipercyclobutanamide B-Mpro (D) showing the main residues that interact through Hbonds (purple arrows), Pi-Pi stacking (green dotted line), polar attractions (light-blue residues and contour), and hydrophobic interactions (light-green residues and contour). Protein ribbons representations showing the binding region of N3-I (B) and pipercyclobutanamide B (E), close to the Mpro beta-barrel motif. Protein surface representations showing the 3D configuration of the SARS-CoV-2 Mpro pocket and N3-I (C) and pipercyclobutanamide B (F).

Table 2. Interacting residues of Mpro, RdRp, and human ACE2 with their native inhibitors and best-docked alkamides and piperamides.

Protein	Ligand	Residues in contact	Residues in contact through a H-bond
Mpro	N3-I	Gln-189, Gly-143, His-41, Glu-166, Arg-188, Asp-187, Asp-48, Glu-47, Ser-46, Thr-45, Cys-145 and Tyr-118	Gln-189 and Gly-143
	Pipercyclobutanamide B	Gln-189, Arg-188, Thr-190, His-41, Cys-44, Val-42, Met-165, Phe-140 and Leu-141	Gln-189
RdRp	GS-441524-TPP	Arg-553, Cys-622, Lys-621, Mg-1004, Asn-691, Asp-452, Thr-556, Arg-555, Arg-553, Lys-551, Arg-624 and Asp-623	Arg-553, Cys-622 and Lys-621
	8,9-dihydropiplartine	Mg-1004, Cys-622 and Ala-688	-
ACE2	DCBICA	Arg-273, His-505, His-345, Glu-375, Tyr-515, Arg-518, His-374, Zn-803, Glu-375,	Arg-273, His-505, His-345, Glu-375 and Tyr-515

		Arg-273, Arg-514, Phe-512 and Tyr-510	
	Pipercyclobutanamide B	Ala-348, Thr-371, Zn-803, Arg-518, Glu-145, His-345, Thr-445, His-378, Thr-365, Lys-363, Thr-362, Cys-344, Phe-274, Cys-361 and Met-360	Ala-348 and Thr-371

The dimeric piperamides in the *Piper* genus,[28,29] has DS similarities to N3-I. Particularly, pipercyclobutanamides A and B have the highest DS and therefore the highest potential to interfere with Mpro. Both, N3-I and pipercyclobutanamide B dock through an Hbond to Gln-189 and polar interactions to Arg-188. Pipercyclobutanamide B stabilizes in the same pocket that N3-I, but with some differences due to polarity. The amino acids involved in the stabilization of N3-I and pipercyclobutanamide B are also involved in the interaction with other Mpro inhibitors such as rutin, ritonavir, emetine, and hesperidin.[30] As expected, N3-I binds to the crucial catalytic residues His-41 and Cys-145.[12] However, pipercyclobutanamide B interacts only with His-41 through polar-hydrophobic interactions between the

imidazole group of His-41 and the piperidine-carbonyl-enyl moiety of pipercyclobutanamide B. As shown in Figure 1 and Table 2, N3-I and pipercyclobutanamide B also interact with other important residues of the active site such as Met-49, Gly-143, His-163, His-164, Glu-166 and Pro-168.[13,18]

The higher DS value of pipercyclobutanamide B over N3-I could be due to the interactions with the protein residues or the 3D configuration. Pipercyclobutanamide B has an X-form conformation that docks in an X-form protein pocket, (Figure 1D-F). Pipercyclobutanamides A and B are considered trace constituents of black peppercorns (*Piper nigrum*) with less than 0.12% and 0.006% by dry weight, respectively.[28] However, these compounds can be fully synthesized.[31,32] To our knowledge, this is the first report of dimeric-piperamides, specifically the pipercyclobutanamides, as potential antivirals via inhibition of SARS-CoV-2 Mpro.

The best-docked ligand against SARS-CoV-2 RdRp was the triphosphate form of GS-441524 (DS = -8.495 Kcal/mol), the metabolically derived RdRp native inhibitor from Remdesivir. None of the analyzed compounds reach 70% of the inhibitor DS value (Table 1). However, some compounds with considerable DS (60% of GS-

441524-TPP DS) were the 8,9-dihydropiplartine (DS = -5.432 Kcal/mol), the pipercyclobutanamide A (DS = -5.417 Kcal/mol) and the *cis*-piplartine (DS = -5.073 Kcal/mol). TPP-GS-441524 assembles into the pocket of the active site (Figure 2A-C) whereas the 8,9-dihydropiplartine molecule docks deeper into the pocket of the active site of SARS-CoV-2 RdRp (Figures 2D-F). The interaction between the residues of RdRp and TPP-GS-441524 and 8,9-dihydropiplartine is reported in Table 2.

The molecular docking results showed that alkamides and piperamides are less effective against the SARS-CoV-2 RdRp compared to SARS-CoV-2 Mpro. The alkamides/piperamides DS values do not reach that of the SARS-CoV-2 RdRp native inhibitor because of the triphosphate moiety in the GS-441524-TPP and its mimicry with the nucleotide triphosphates that are the RdRp native ligands. Also, the crystalized structure of RdRp shows that the Hbonds to Arg-553, Thr-687 and Asp-760 are important for its catalytic activity.[33] In the crystalized structure, the triphosphate moiety is hydrolyzed into 2-pyrophosphate and the monophosphate-inhibitor form. Arg-553 forms two Hbonds to the beta-phosphate of the free 2-

pyrophosphate, Asp-760 forms two Hbonds to the bonded alfa-monophosphate and Thr-687 forms one more Hbond to the hydroxy group at the cyano-oxolane moiety.[33] After redocking, the triphosphate form of the inhibitor the phosphate groups remained as the docking points. The anchor residues change in the interaction importance since only Arg-553 remains to form an Hbond and Cys-622 along with Lys-621 binds via Hbonds to the beta-phosphate group. As expected, interactions with Mg-1004 are present in both crystalized and redocked inhibitor-protein complexes.[33]

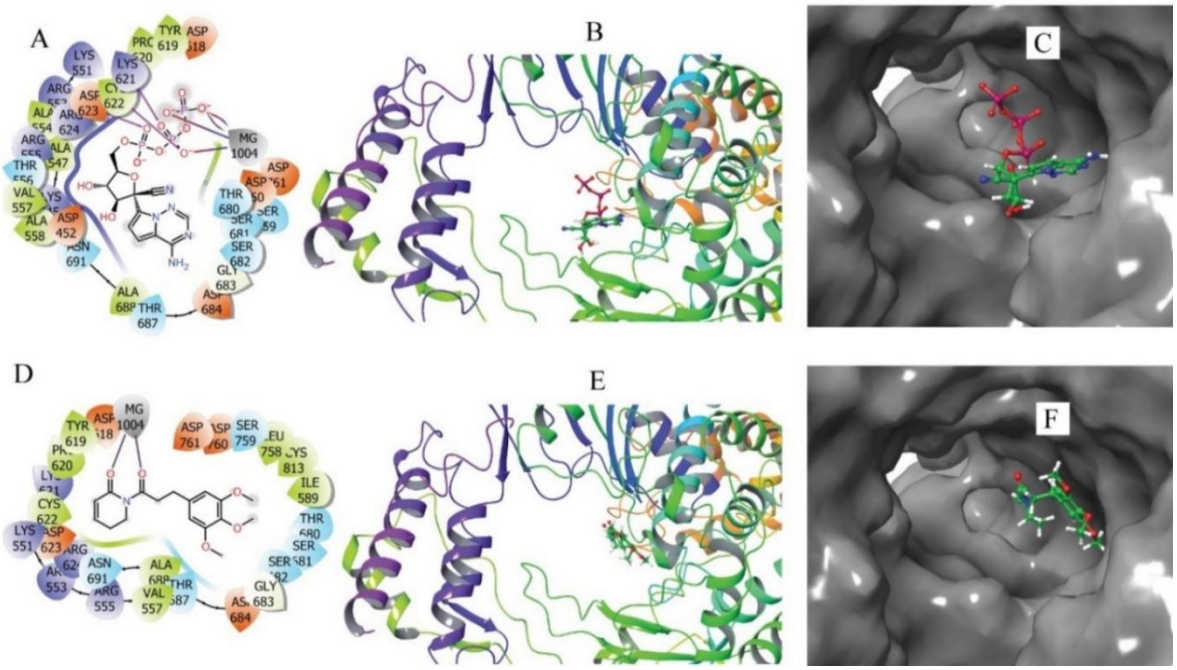

Figure 2. Molecular docking for SARS-CoV-2 RdRp against GS-441524-TPP (A, B, C) and 8,9-dihydropiplartine (D, E, F). Interaction representations of the complexes GS-441524-TPP-RdRp (A) and 8,9-dihydropiplartine-RdRp (D) showing the main residues that interact through Hbonds (purple arrows), Pi-Pi stacking (green dotted line), polar attractions (light-blue residues and contour), and hydrophobic interactions (light-green residues and contour). Protein ribbons representations showing the binding region of GS-441524-TPP (B) and 8,9-dihydropiplartine (E), in the active site across the RdRp synthetic channel. Protein surface representations showing the 3D configuration of the SARS-CoV-2 RdRp pocket and GS-441524-TPP (C) and 8,9-dihydropiplartine (F).

The tested compounds fail to reach a comparable DS to the SARS-CoV-2 RdRp inhibitor. However, some piperamides (present in *Piper tuberculatum* [34]) had sufficient DS to warrant future research. The 8,9-dihydropiplartine and pipercyclobutanamide A were the best-docked compounds with similar DS. Both compounds coordinate with the Mg-1004 through the carbonyl moiety of the amide

groups. No important interactions are formed to the catalytic Arg-553, Thr-687 and Asp-760, but the proximity of these residues to Pi-electrons could be contributing to the DS of 8,9-dihydropiplartine and pipercyclobutanamide A. The lower DS of the alkamides is due to the different size and configuration compared to the docked SARS-CoV-2 RdRp inhibitor and the native ligands, however, 8,9-dihydropiplartine and pipercyclobutanamide A docked in the active site. The phosphate groups are important in the search for effective inhibitors of RdRp polymerase, as previously documented. Therefore, future research on non-nucleoside inhibitors should include the development of alkamide-phosphate like compounds with piperamide moieties. The use of *P. tuberculatum* or 8,9 dihydropiplartine as antivirals has not been previously reported.

As expected, the best ligand against human ACE2 was the native inhibitor DCBICA (DS = -10.558 Kcal/mol). Some of the tested compounds docked with considerable DS (65% of DCBICA): the pipercyclobutanamide B (DS = -7.34 Kcal/mol), the pipercyclobutanamide A (DS = -6.997 Kcal/mol) and the nigramide Q (DS = -6.855 Kcal/mol). Carboxylic groups of DCBICA are involved in most of these interactions

as seen in Figure 3A. The DCBICA molecule docks into the pocket of the active site duct (Figure 3B-C). Pipercyclobutanamide B fits in the pocket along internal ducts around the active site (Figures 3D-F). The interactions between the residues of ACE2 and DCBICA and pipercyclobutanamide B are reported in Table 2.

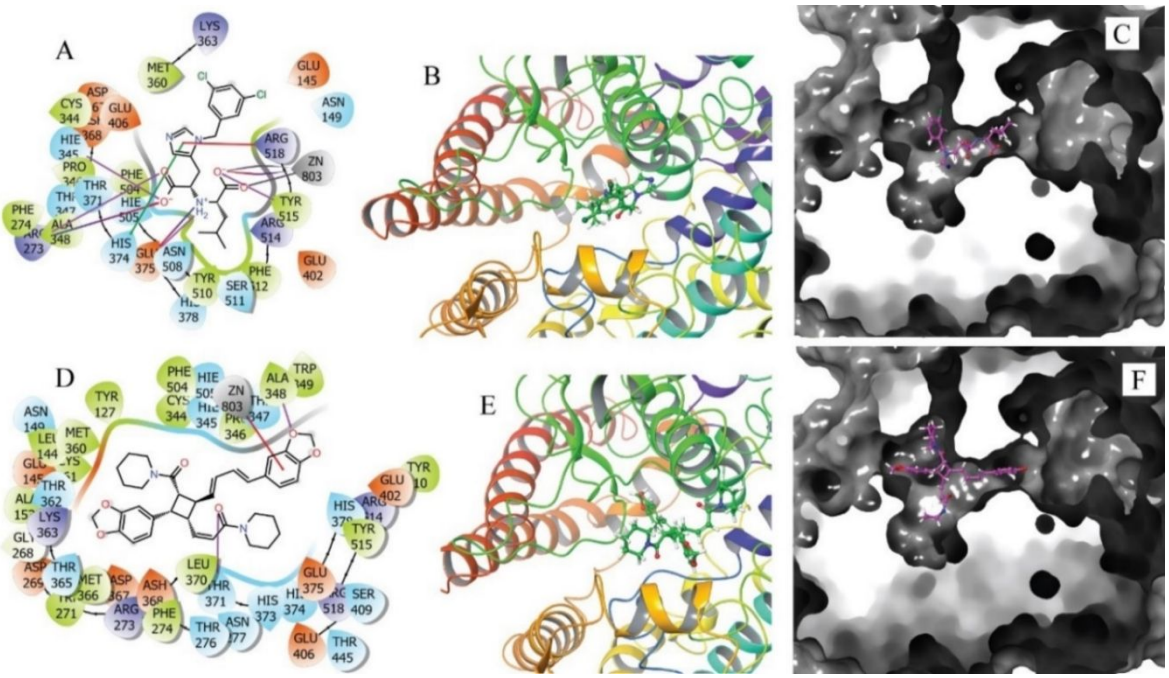

Figure 3. Molecular docking for human ACE2 against DCBICA (A, B, C) and pipercyclobutanamide B (D, E, F). Interaction representations of the complexes DCBICA-ACE2 (A) and pipercyclobutanamide B-ACE2 (D) showing the main residues that interact through Hbonds (purple arrows), Pi-Pi stacking (green dotted

line), polar attractions (light-blue residues and contour), and hydrophobic interactions (light-green residues and contour). Protein ribbons representations showing the binding region of DCBICA (B) and pipercyclobutanamide B (E), in the active site inside the ACE2 alfa-helix barrels that form the protein body. Protein surface representations showing the 3D configuration of human ACE2 pocket and DCBICA-ACE2 (C) and pipercyclobutanamide B-ACE2 (F). The cross-section view shows the channel entrance-size.

The DS value of the DCBICA-human ACE2 complex was the highest overall, showing that DCBICA is a strong inhibitor of human ACE2. Similar to the SARS-CoV-2 Mpro and RdRp results, some piperamides could also be potential inhibitors of ACE2. No comparable residue interactions between the DCBICA and the piperamides ACE2-complexes were identified, reflecting their low DS. The considerable DS of piperamides could be due to the attachment between the 3D configuration of the docked ligands and the 3D configuration of the human ACE2

pocket. The protein pocket entrance-size also needs to be considered. Although the best-docked piperamides bound with regular DS, they may be too large to enter the human ACE2 pocket. In that case, other non-dimeric alkamides or pipermides with lower DS and smaller size could be investigated (Table 1; i.e. *N*-isobutyl-(2*E*,4*Z*)-octadienamide and the *N*-(2-phenylethyl)-*cis*-2,3-epoxynona-6,8-diynamide).

The absorption, distribution, metabolism and excretion (ADME) properties of the native inhibitors and the tested compounds with the highest DS for each protein are listed in Table 3. According to their molecular properties, Lipinski's rule of 5 (RO5) was used to evaluate the potential of these alkamides as orally active drugs in humans.[35] Additionally, the Jorgensen rule of 3 (RO3) was used to evaluate the oral availability of the compounds.[36] The violations to the RO5 and RO3 are listed in Table 3. The dimeric piperamides violate the rules of maximum molecular weight and/or permeability. However, they performed better than N3-I and GS-441524-TPP. Therefore, these piperamides have considerable drug potential, especially considering their favourable traits such as high oral absorption, brain/blood partition

coefficient, predicted binding to human serum albumin, and activity in the central nervous system (Table 3).

Table 3. ADME profile of selected alkamides and piperamides.

Number	MW	DonorHB /AccptHB	Human Oral Absorption	QPlogo/w	QPlogS	QPlogBB	QPlogKhsa	CNS	RO5/RO3
4	251.3	1/1	High	4.25	-4.75	-0.34	0.44	0	0/0
48	532.6	1/1	High	3.93	-4.79	0.00	0.21	0	1/0
49	446.7	2/2	Low	6.38	-8.26	-0.76	0.94	-1	1/1
50	446.7	2/2	Low	6.49	-7.00	-1.11	1.16	-2	1/1
56	544.6	0/0	Low	4.58	-6.30	-0.13	0.39	-1	1/1
57	544.6	0/0	High	3.89	-4.56	-0.04	-0.05	-1	1/0
58	570.7	0/0	High	4.87	-5.36	-0.13	0.38	-1	1/0

59	596.7	0/0	Low	5.83	-6.89	-0.26	0.72	-1	2/1
62	319.4	0/5.25	High	3.32	-4.54	-0.81	0.13	-1	0/0
64	317.3	0/5.25	High	2.92	-3.97	-0.43	-0.13	0	0/0
98	680.8	2.75/13.75	Low	2.84	-6.03	-4.03	-0.40	-2	2/3
99	531.2	4/19.65	Low	-1.82	-1.76	-5.25	-2.53	-2	3/1
100	428.3	3/7	Low	1.91	-4.58	-1.28	-0.15	-2	0/1

ID = Identification number according to Table 1. ADME parameters: MW = molecular weight, DonorHB = number of Hbonds donors, AccptHB = number of Hbonds acceptors, QPlogo/w = octanol/water partition coefficient, QPlogS = predicted aqueous solubility, QPlogBB = brain/blood partition coefficient, QPlogKhsa = prediction of binding to human serum albumin, CNS = predicted central nervous system activity on a –2 (inactive) to +2 (active) scale, RO5 = number of violations to rule of five, RO3 = number of violations to rule of three.

We used MD simulations to explore the evolution of the complex ligand-Mpro through time. MD analysis is a very computationally demanding process, hence we selected pipercyclobutanamide B, the piperamide with the best docking results, and

the native inhibitor (N3-I) for the analysis. The MD simulations results show that the N3-I binds stably to the Mpro active site residues (Figure 4A, Table 4, Table S2). Similarly, the same Mpro residues in contact with the pipercyclobutanamide B maintained low RMSD changes; except for the 188 and 189 residues that increased their RMSD movement at the last nanosecond of the MD simulation (Figure 4B, Table 4, Table S3). During the MD simulation, Mpro-ligand complexes were able to maintain low ligand movement below 3.5 Å and stabilizing at an average of 2.5 Å after 1 ns. This indicates proximity and stronger binding for both compounds to the Mpro active site (Figure 4C). Protein movement RMSD stabilizes around 1.5 Å after 2 ns for both ligands, following similar trajectories (Figure 4D). Additionally, small conformational changes were observed for protein and ligands during MD simulation (Figure 4 E-F). The active site residues contact number for Mpro-N3-I and Mpro-pipercyclobutanamide B complexes show a similar level of protein-ligand interaction during the simulation for both ligands (Figure 4G).

A contact between two molecules is defined when the heavy atom of one molecule is within a cutoff distance from the heavy atom of another molecule.[37] The contact

fingerprint of Mpro with pipercyclobutanamide B shows that during the 5.5 ns of the MD simulation, the ligand had contacts with all the heavy atoms from the protein backbone with most of the amino acids that form the binding pocket (Figure 4G). In average, pipercyclobutanamide B contacts increased with Glu-166, His-163 and Asn-142 compared to N3-I (Figure 4G), amino acids that belong to the binding pocket subunit S1.[12] Ligand-protein interactions with aminoacids in the subunit S1 such as Glu-166 and His-163 are important interactions with inhibitors like cinancerin, nelfinavir, pralmorelin and N3.[12,38] Also, the residue His-41 that belongs to the Mpro catalytic dyad increased the number of contacts as well as Met-49, Met-165 and Asp-187 that belongs to the binding pocket subsite S2,[12] while Cyst-145 contacts remain similar as N3-I (Fig. 4G).

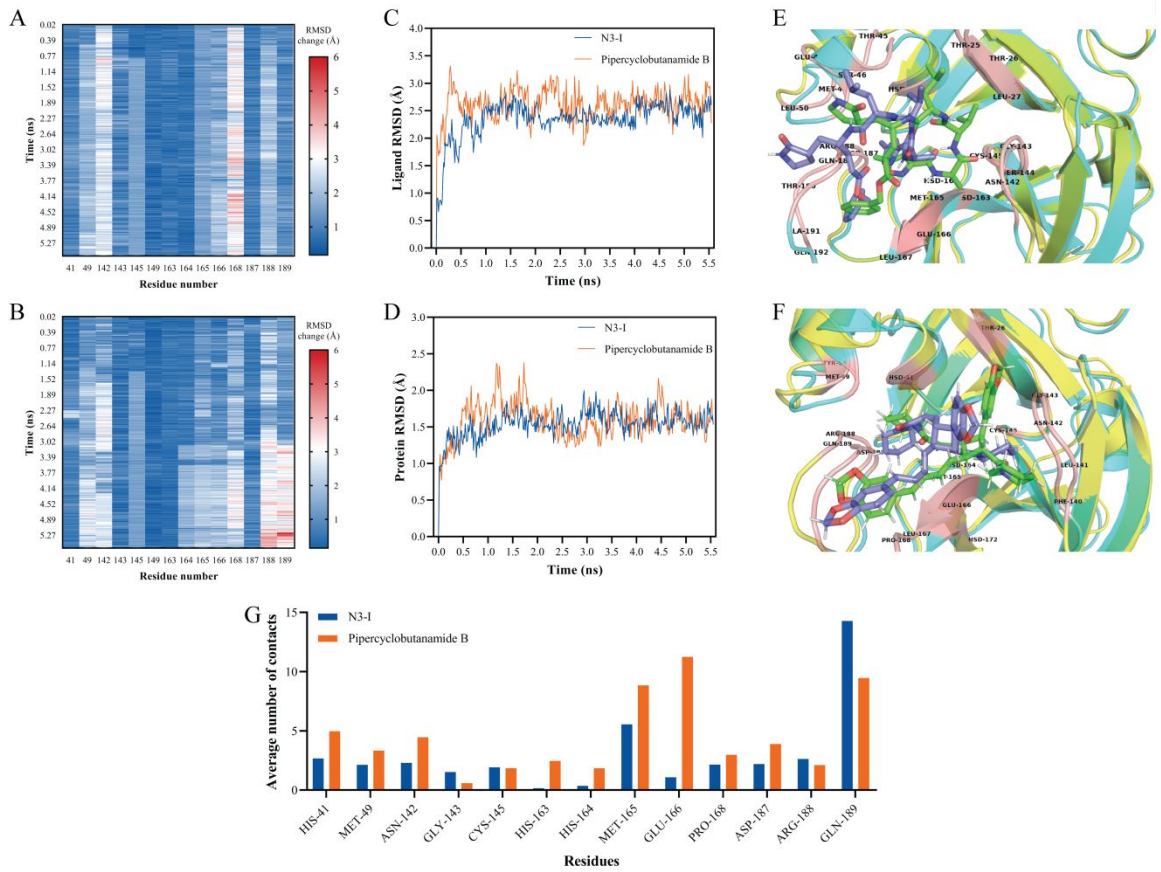

Figure 4. Molecular dynamics for Mpro-N3-I and Mpro-pipercyclobutanamide B complex. Heatmap plots of RMSD changes for binding pocket amino acid residues in the Mpro-N3-I (A) and Mpro-pipercyclobutanamide B (B) during 5.5 ns of simulation. The color key ranges from the smallest movements in blue to the largest movements in dark red. Ligands movement RMSD after complexing with Mpro during 5.5 ns of MD simulation (C). Mpro protein backbone movement RMSD after complexing with the respective ligand during 5.5 ns of MD simulation (D). RMSD values were calculated as the deviation from the initial structure models at 0 ns.

Representation of the differences in structural conformation of N3-I (E) and pipercyclobutanamide B (F) from beginning to the end of the simulation. Average protein-ligand contact analysis during MD simulations for N3-I and pipercyclobutanamide B (G).

Table 4. Root-mean-square deviation of atomic positions (RMSD) for the Mpro catalytic residues 41 and 145 obtained from molecular dynamics simulation for Mpro-N3-I and Mpro-Pipercyclobutanamide B complexes. RMSD values are shown in Å.

Mpro Residue	RMSD change for Mpro - N3-1 complex			RMSD change for Mpro - Pipercyclobutanamide B complex		
	Mean	Max	Min	Mean	Max	Min
41	1.040	1.953	0.411	0.968	2.987	0.297
145	1.423	1.907	0.170	1.352	1.915	0.241

The molecular docking results for SARS-CoV-2 Mpro and RdRp, and human ACE2 indicate that some alkamides and piperamides have high antiviral potential against SARS-CoV-2, especially, the dimeric piperamides of *Piper nigrum* and *Piper chaba*.

The phenethyl-alkamides found in the *Acmella* genus may also interact considerably with these three proteins. The capsaicinoids of the *Capsicum* genus and major piperamides of *P. nigrum* (piperine and trichostachine) affect RdRp in particular. The potential anti-SARS-CoV-2 activity of the tested compounds is linked mainly to interference with the Mpro function. Therefore, the effect of piperine-enriched essential oils of *Piper* species and piperamide-like purified compounds should be examined *in vitro* and *in vivo*. The ADME studies further support the anti-SARS-CoV-2 potential of the dimeric piperamides from *Piper* species, primarily against the main protease (Mpro) of SARS-CoV-2, but also considerably against SARS-CoV-2 RdRp and the human ACE2. The MD simulations showed that pipercyclobutanamide B forms a complex with Mpro with similar stability to N3-I, indicating promising performance for future *in vitro* and *in vivo* experiments. Then, piperamides and related compounds should be considered for a possible alkamide/piperamide-based treatment. Many of the examined compounds have common culinary uses, including the piperamides and capsaicinoids found in the common pepper (*P. nigrum*) and chili pepper (*Capsicum annuum*), respectively. Possible mitigating effects of an

alkamide/piperamide-rich diet on coronavirus susceptibility should be studied. Based on past and herein presented data, amide-aromatic-like natural products could potentially act as antivirals against SARS-CoV-2 and related coronaviruses. These results show the potential of dimeric piperamides, specifically the pipercyclobutanamide B, as potential antivirals against SARS-CoV-2.

Experimental Methods

The SARS-CoV-2 Mpro (PDB ID: 6LU7; resolution 2.14 Å),[12] the SARS-CoV-2 RdRp (PDB ID: 7BV2; resolution 2.5 Å),[33] and the Human ACE2 (PDB ID: 1R4L; resolution 3 Å)[39] protein crystal structures were retrieved from the Protein Data Bank (www.rcsb.org/). The Mpro chain A (306 amino acids) of the structure was prepared using the Protein Preparation Wizard and the Virtual Screening Workflow tools of Maestro Schrödinger software.[25,40] The protein states were generated at pH of 7.0 ± 0.5 and H-bonds were optimized using “sample water orientations” option at pH of 7.0 after deleting the ligated inhibitor N3-I (N-[(5-Methyl-1,2-oxazol-3-yl)carbonyl]-L-alanyl-L-valyl-N-{(2S,3E)-5-(benzyloxy)-5-oxo-1-[(3S)-2-oxo-3-pyrrolidinyl]-3-

penten-2-yl}-L-leucinamide). States were minimized converging heavy atoms to RMSD of 0.3 Å and an OPLS3e option force field. All other parameters were set to default values. The RdRp and ACE2 proteins were prepared following the same steps as for 6LU7 but with the following considerations. For 7BV2, only the chain A (888 amino acids) was used and the RNA molecule was deleted to avoid incorrect interactions during docking simulations. For 1R4L, the chain A (782 amino acids) was used. Each protein was prepared on a separate project to facilitate the results inspection.

Based on published literature and to cover a variety of chemical structures, 97 alkamides and piperamides were selected and retrieved from PubChem. The structures of the Mpro, RdRp, and ACE2 inhibitors were retrieved from PubChem. All structures are listed on Supplemental Table 1, including their respective PubChem ID. All ligands were prepared by generating states at a pH of 7.0 with desalt and generating tautomers options. There were generated for each ligand at most 32 possible states using the OPLS3e force field option.[25] The compounds that did not have interaction with Mpro, RdRp and ACE2 were not included in the result

Table 1. However, they were included in the Supporting Information Table 1, since negative results have a scientific value.

The molecular docking was performed between each protein and ligand using the Grid-Based Ligand Docking with Energetics (GLIDE) module of Maestro Schrödinger software. The grids for each protein was generated using the Grid Generation tool.[25,41–43] The grid box of processed-6LU7 was centred at the same coordinates of the crystallized ligand (x:-1074, y:10.36, z:68.95), previously deleted. For processed-7BV2, the grid box was centered by picking on the ligated inhibitor GS-441524 triphosphate ((2R,3R,4S,5R)-2-(4-Aminopyrrolo[2,1-f][1,2,4]triazin-7-yl)-3,4-dihydroxy-5-(hydroxymethyl)oxolane-2-carbonitrile-TPP) at x:91.74, y:92.43, z:103.75. For processed-1R4L the grid box was centered by picking on the ligated inhibitor DCBICA ((S,S)-2-{1-Carboxy-2-[3-(3,5-dichloro-benzyl)-3H-imidazol-4-YL]-ethylamino}-4-methyl-pentanoic acid) at x:40.61, y:5.82, z:27.84. Each ligand was docked into each protein, based on the respective grid, using standard precision (SP) docking algorithm with flexible ligand sampling option.[25,41–43] The Qik-Prop[44]

module of Maestro Schrödinger was used to determine the ADME profile of the alkamides with the highest docking score for the respective protein.

Molecular Dynamics simulations were run using the Large-scale Atomic/Molecular Massively Parallel Simulator code (LAMMPS) and using CHARMM36 additive force field for protein as well as protein-ligand complexes.[45,46] The system was minimized with the Polak-Ribiere version of the conjugate gradient (CG) algorithm and then equilibrated applying bond and angle constraints to specified bonds and angles in the simulation with the SHAKE algorithm[47] and the canonical NVT ensemble. The production of MD simulations were performed at a constant temperature of 310.15 °K and a constant pressure of 0.986 bars using the isothermal–isobaric ensemble (constant temperature and constant pressure ensemble). All the simulations input scripts were generated with the CHARM-GUI Solution Builder.[48,49] To generate the input files for simulations and prepare the solvent system we used the interactive web-based platform CHARMM-GUI.[50] The protein-ligand complexes were placed in an octahedral waterbox with 5.0 Å of edge distance, 0.1 M KCl ions and Monte-Carlo ion placing method.[48] The simulations were conducted for 5.55 ns and performed on

a workstation with Windows 10 Pro 64 bits, AMD Threadripper 1950X, 16 cores, 64 GB RAM. The stability of the protein and protein-ligand complex system was analyzed by calculating the root mean square deviation (RMSD) and root mean square fluctuation (RMSF) using the Bio3d package in R-Studio.[51,52] A contact analysis between the residues in the binding pocket (residues 40-190) and the corresponding ligand was made with the Timeline plugin (V.2.3) in the Visual Molecular Dynamics (VMD) software and the heatmaps were constructed with the data matrix extracted from the RMSD Visualizer Tool plugin in VMD. The RcolorBrewer pallet was used to assign color blind-friendly colors to the graphs.[53]

ASSOCIATED CONTENT

Supporting Information. This material is available free of charge via the Internet at http://pubs.acs.org.

The following files are available free of charge.

A Table is provided with the docking scores, PubChem accession number, and other chemical properties of the alkamides herein analyzed (PDF).

An excel file is provided with the RMSD changes.

A file with the optimized structures is provided.

An excel file is provided with the molecular formula strings.

AUTHOR INFORMATION

Corresponding Author

* Juan Vázquez-Martínez – Instituto Tecnológico Superior de Irapuato, TecNM, 36821, Irapuato, Guanajuato, México; orcid.org/0000-0002-3037-1457;

E-mail: juan.vazquez@itesi.edu.mx

Author Contributions

Juan Manuel Gutierrez-Villagomez: Conceptualization, software, investigation, data curation, writing original draft, writing review and editing. Tonatiu Campos García: Software, investigation, data curation, writing, review and editing. Jorge Molina-Torres: validation, formal analysis, writing review and editing. Mercedes G. López: validation, formal analysis, writing review and editing. Juan Vázquez-Martínez: Conceptualization, methodology, data curation, writing original draft, writing review

and editing, supervision, validation, resources, project administration and funding acquisition. The manuscript was written through contributions of all authors. All authors have approved the final version of the manuscript.

Funding Sources

The authors would like to thank SNI-CONACyT, ITESI and CINVESTAV-Irapuato for support.

ACKNOWLEDGMENT

We would like to thank Wo Su Zhang and Enrique Ramírez-Chávez for proofreading and providing helpful feedback that improved the manuscript. We acknowledge with appreciation the computational support from Dr. Frederick Ayala-Gómez.

ABBREVIATIONS

SARS-CoV, severe acute respiratory syndrome coronavirus; MERS-CoV, middle east respiratory syndrome coronavirus; SARS-CoV-2, severe acute respiratory

syndrome coronavirus 2; COVID-19, associated syndrome of SARS-CoV-2; Mpro, SARS-CoV-2 main protease; Nsp5, non-structural protein 5; 3CLpro, 3C-like protease; RdRp, RNA-dependent RNA polymerase; Nsp12, non-structural protein 12; ACE2, angiotensin-converting enzyme 2; DS, docking score; Hbond, hydrogen bond; N3-I, *N*-[(5-Methyl-1,2-oxazol-3-yl)carbonyl]-L-alanyl-*L*-valyl-*N*-{(2S,3E)-5-(benzyloxy)-5-oxo-1-[(3S)-2-oxo-3-pyrrolidinyl]-3-penten-2-yl}-L-leucinamide); GS-441524-TPP, (2*R*,3*R*,4*S*,5*R*)-2-(4-Aminopyrrolo[2,1-f][1,2,4]triazin-7-yl)-3,4-dihydroxy-5-(hydroxymethyl) oxolane-2-carbonitrile-triphosphate; DCBICA, (S,S)-2-{1-Carboxy-2-[3-(3,5-dichloro-benzyl)-3H-imidazol-4-YL]-ethylamino}-4-methyl-pentanoic acid); ADME, favorable absorption, distribution, metabolism and excretion.

REFERENCES

(1) Paules, C. I.; Marston, H. D.; Fauci, A. S. Coronavirus Infections-More Than Just the Common Cold. *JAMA* **2020**.

(2) Peiris, J. S. M.; Lai, S. T.; Poon, L. L. M.; Guan, Y.; Yam, L. Y. C.; Lim, W.;

Nicholls, J.; Yee, W. K. S.; Yan, W. W.; Cheung, M. T.; et al. Coronavirus as a Possible Cause of Severe Acute Respiratory Syndrome. *Lancet (London, England)* **2003**, *361* (9366), 1319–1325.

(3) Zaki, A. M.; van Boheemen, S.; Bestebroer, T. M.; Osterhaus, A. D. M. E.; Fouchier, R. A. M. Isolation of a Novel Coronavirus from a Man with Pneumonia in Saudi Arabia. *N. Engl. J. Med.* **2012**, *367* (19), 1814–1820.

(4) Zhu, N.; Zhang, D.; Wang, W.; Li, X.; Yang, B.; Song, J.; Zhao, X.; Huang, B.; Shi, W.; Lu, R.; et al. A Novel Coronavirus from Patients with Pneumonia in China, 2019. *N. Engl. J. Med.* **2020**, *382* (8), 727–733.

(5) Zhang, L.; Lin, D.; Kusov, Y.; Nian, Y.; Ma, Q.; Wang, J.; von Brunn, A.; Leyssen, P.; Lanko, K.; Neyts, J.; et al. Alpha-Ketoamides as Broad-Spectrum Inhibitors of Coronavirus and Enterovirus Replication: Structure-Based Design, Synthesis, and Activity Assessment. *J. Med. Chem.* **2020**, *63* (9), 4562–4578.

(6) Johns Hopkins University. Johns Hopkins Coronavirus Resource Center https://coronavirus.jhu.edu/map.html (accessed Aug 11, 2020).

(7) World Health Organization. Coronavirus https://www.who.int/health-topics/coronavirus#tab=tab_1 (accessed May 18, 2020).

(8) World Health Organization. Coronavirus: Symptoms https://www.who.int/health-topics/coronavirus#tab=tab_3 (accessed May 18, 2020).

(9) Milken Institute. COVID-19 Treatment and Vaccine Tracker https://milkeninstitute.org/covid-19-tracker?fbclid=IwAR0GNbaklsHB-Y9YNj7t-u9oeAK24RwUsl6leBYJxCVozmVyU6n3lK7qT14 (accessed May 18, 2020).

(10) Zhang, L.; Lin, D.; Sun, X.; Curth, U.; Drosten, C.; Sauerhering, L.; Becker, S.; Rox, K.; Hilgenfeld, R. Crystal Structure of SARS-CoV-2 Main Protease Provides a Basis for Design of Improved Alpha-Ketoamide Inhibitors. *Science* **2020**, *368* (6489), 409–412.

(11) Wang, F.; Chen, C.; Tan, W.; Yang, K.; Yang, H. Structure of Main Protease from Human Coronavirus NL63: Insights for Wide Spectrum Anti-Coronavirus Drug Design. *Sci. Rep.* **2016**, *6*, 22677.

(12) Jin, Z.; Du, X.; Xu, Y.; Deng, Y.; Liu, M.; Zhao, Y.; Zhang, B.; Li, X.; Zhang, L.; Peng, C.; et al. Structure of M(pro) from SARS-CoV-2 and Discovery of Its Inhibitors. *Nature* **2020**.

(13) Wang, J. Fast Identification of Possible Drug Treatment of Coronavirus Disease-19 (COVID-19) through Computational Drug Repurposing Study. *J. Chem. Inf. Model.* **2020**.

(14) Ko, W.-C.; Rolain, J.-M.; Lee, N.-Y.; Chen, P.-L.; Huang, C.-T.; Lee, P.-I.; Hsueh, P.-R. Arguments in Favour of Remdesivir for Treating SARS-CoV-2 Infections. *International journal of antimicrobial agents*. Netherlands April 2020, p 105933.

(15) Elfiky, A. A. Ribavirin, Remdesivir, Sofosbuvir, Galidesivir, and Tenofovir against SARS-CoV-2 RNA Dependent RNA Polymerase (RdRp): A Molecular Docking Study. *Life Sci.* **2020**, *253*, 117592.

(16) Donoghue, M.; Hsieh, F.; Baronas, E.; Godbout, K.; Gosselin, M.; Stagliano, N.; Donovan, M.; Woolf, B.; Robison, K.; Jeyaseelan, R.; et al. A Novel Angiotensin-Converting Enzyme-Related Carboxypeptidase (ACE2) Converts

Angiotensin I to Angiotensin 1-9. *Circ. Res.* **2000**, *87* (5), E1-9.

(17) Hamming, I.; Timens, W.; Bulthuis, M. L. C.; Lely, A. T.; Navis, G. J.; van Goor, H. Tissue Distribution of ACE2 Protein, the Functional Receptor for SARS Coronavirus. A First Step in Understanding SARS Pathogenesis. *J. Pathol.* **2004**, *203* (2), 631–637.

(18) Kumar, D.; Chandel, V.; Raj, S.; Rathi, B. In Silico Identification of Potent FDA Approved Drugs against Coronavirus COVID-19 Main Protease: A Drug Repurposing Approach. *Chem. Biol. Lett. Vol 7, No 3* **2020**.

(19) Thuy, B. T. P.; My, T. T. A.; Hai, N. T. T.; Hieu, L. T.; Hoa, T. T.; Thi Phuong Loan, H.; Triet, N. T.; Anh, T. T. Van; Quy, P. T.; Tat, P. Van; et al. Investigation into SARS-CoV-2 Resistance of Compounds in Garlic Essential Oil. *ACS omega* **2020**, *5* (14), 8312–8320.

(20) Verdecchia, P.; Angeli, F.; Reboldi, G. Angiotensin-Converting Enzyme Inhibitors, Angiotensin II Receptor Blockers and Coronavirus. *J. Hypertens.* **2020**, *38* (6), 1190–1191.

(21) Olimat, M. Y. R. E.-O. V. E.-S. M. Natural Alkamides: Pharmacology,

Chemistry and Distribution; IntechOpen: Rijeka, 2012; p Ch. 6.

(22) Rios, M. Y.; Olivo, H. F. Chapter 3 - Natural and Synthetic Alkamides: Applications in Pain Therapy; Atta-ur-Rahman, B. T.-S. in N. P. C., Ed.; Elsevier, 2014; Vol. 43, pp 79–121.

(23) Boonen, J.; Bronselaer, A.; Nielandt, J.; Veryser, L.; De Tre, G.; De Spiegeleer, B. Alkamid Database: Chemistry, Occurrence and Functionality of Plant N-Alkylamides. *J. Ethnopharmacol.* **2012**, *142* (3), 563–590.

(24) Molina-Torres, J.; Garcia-Chavez, A.; Ramirez-Chavez, E. Antimicrobial Properties of Alkamides Present in Flavouring Plants Traditionally Used in Mesoamerica: Affinin and Capsaicin. *J. Ethnopharmacol.* **1999**, *64* (3), 241–248.

(25) Vazquez-Martinez, J.; Buitemea-Cantua, G. V; Gutierrez-Villagomez, J. M.; Garcia-Gonzalez, J. P.; Ramirez-Chavez, E.; Molina-Torres, J. Bioautography and GC-MS Based Identification of Piperine and Trichostachine as the Active Quorum Quenching Compounds in Black Pepper. *Heliyon* **2020**, *6* (1), e03137.

(26) Hernandez, I.; Marquez, L.; Martinez, I.; Dieguez, R.; Delporte, C.; Prieto, S.; Molina-Torres, J.; Garrido, G. Anti-Inflammatory Effects of Ethanolic Extract and Alkamides-Derived from Heliopsis Longipes Roots. *J. Ethnopharmacol.* **2009**, *124* (3), 649–652.

(27) Ramirez-Chavez, E.; Lopez-Bucio, J.; Herrera-Estrella, L.; Molina-Torres, J. Alkamides Isolated from Plants Promote Growth and Alter Root Development in Arabidopsis. *Plant Physiol.* **2004**, *134* (3), 1058–1068.

(28) Fujiwara, Y.; Naithou, K.; Miyazaki, T.; Hashimoto, K.; Mori, K.; Yamamoto, Y. Two New Alkaloids, Pipercyclobutanamides A and B, from Piper Nigrum. *Tetrahedron Lett.* **2001**, *42* (13), 2497–2499.

(29) Rao, V. R. S.; Suresh, G.; Babu, K. S.; Raju, S. S.; Vishnu vardhan, M. V. P. S.; Ramakrishna, S.; Rao, J. M. Novel Dimeric Amide Alkaloids from Piper Chaba Hunter: Isolation, Cytotoxic Activity, and Their Biomimetic Synthesis. *Tetrahedron* **2011**, *67* (10), 1885–1892.

(30) Das, S.; Sarmah, S.; Lyndem, S.; Singha Roy, A. An Investigation into the Identification of Potential Inhibitors of SARS-CoV-2 Main Protease Using

Molecular Docking Study. *J. Biomol. Struct. Dyn.* **2020**, 1–11.

(31) Gutekunst, W. R.; Gianatassio, R.; Baran, P. S. Sequential C□H Arylation and Olefination: Total Synthesis of the Proposed Structure of Pipercyclobutanamide A. *Angew. Chemie Int. Ed.* **2012**, *51* (30), 7507–7510.

(32) Liu, R.; Zhang, M.; Wyche, T. P.; Winston-McPherson, G. N.; Bugni, T. S.; Tang, W. Stereoselective Preparation of Cyclobutanes with Four Different Substituents: Total Synthesis and Structural Revision of Pipercyclobutanamide A and Piperchabamide G. *Angew. Chemie Int. Ed.* **2012**, *51* (30), 7503–7506.

(33) Yin, W.; Mao, C.; Luan, X.; Shen, D.-D.; Shen, Q.; Su, H.; Wang, X.; Zhou, F.; Zhao, W.; Gao, M.; et al. Structural Basis for Inhibition of the RNA-Dependent RNA Polymerase from SARS-CoV-2 by Remdesivir. *Science* **2020**.

(34) Cotinguiba, F.; Regasini, L. O.; da Silva Bolzani, V.; Debonsi, H. M.; Duó Passerini, G.; Cicarelli, R. M. B.; Kato, M. J.; Furlan, M. Piperamides and Their Derivatives as Potential Anti-Trypanosomal Agents. *Med. Chem. Res.* **2009**, *18* (9), 703.

(35) Lipinski, C. A.; Lombardo, F.; Dominy, B. W.; Feeney, P. J. Experimental and Computational Approaches to Estimate Solubility and Permeability in Drug Discovery and Development Settings. *Adv. Drug Deliv. Rev.* **1997**, *23* (1), 3–25.

(36) Schrödinger Press. QikProp 3.4 User Manual. *LLC, New York, NY* **2011**.

(37) Berrera, M.; Molinari, H.; Fogolari, F. Amino Acid Empirical Contact Energy Definitions for Fold Recognition in the Space of Contact Maps. *BMC Bioinformatics* **2003**, *4* (1), 8.

(38) Kanhed, A. M.; Patel, D. V; Teli, D. M.; Patel, N. R.; Chhabria, M. T.; Yadav, M. R. Identification of Potential Mpro Inhibitors for the Treatment of COVID-19 by Using Systematic Virtual Screening Approach. *Mol. Divers.* **2020**, 1–19.

(39) Towler, P.; Staker, B.; Prasad, S. G.; Menon, S.; Tang, J.; Parsons, T.; Ryan, D.; Fisher, M.; Williams, D.; Dales, N. A.; et al. ACE2 X-Ray Structures Reveal a Large Hinge-Bending Motion Important for Inhibitor Binding and Catalysis. *J. Biol. Chem.* **2004**, *279* (17), 17996–18007.

(40) Schrödinger. Maestro. *Schrödinger, LLC, New York, NY*. 2020.

(41) Schrödinger. Glide. *Glide Schrödinger LLC NY*. 2020.

(42) Friesner, R. A.; Banks, J. L.; Murphy, R. B.; Halgren, T. A.; Klicic, J. J.; Mainz, D. T.; Repasky, M. P.; Knoll, E. H.; Shelley, M.; Perry, J. K.; et al. Glide: A New Approach for Rapid, Accurate Docking and Scoring. 1. Method and Assessment of Docking Accuracy. *J. Med. Chem.* **2004**, *47* (7), 1739–1749.

(43) Halgren, T. A.; Murphy, R. B.; Friesner, R. A.; Beard, H. S.; Frye, L. L.; Pollard, W. T.; Banks, J. L. Glide: A New Approach for Rapid, Accurate Docking and Scoring. 2. Enrichment Factors in Database Screening. *J. Med. Chem.* **2004**, *47* (7), 1750–1759.

(44) Schrödinger. QikProp. *New York, NY*. 2020.

(45) Plimpton, S. Fast Parallel Algorithms for Short-Range Molecular Dynamics. *J. Comput. Phys.* **1995**, *117* (1), 1–19.

(46) Fiorin, G.; Klein, M. L.; Hénin, J. Using Collective Variables to Drive Molecular Dynamics Simulations. *Mol. Phys.* **2013**, *111* (22–23), 3345–3362.

(47) Ryckaert, J.-P.; Ciccotti, G.; Berendsen, H. J. C. Numerical Integration of the Cartesian Equations of Motion of a System with Constraints: Molecular

Dynamics of n-Alkanes. *J. Comput. Phys.* **1977**, *23* (3), 327–341.

(48) Lee, J.; Cheng, X.; Swails, J. M.; Yeom, M. S.; Eastman, P. K.; Lemkul, J. A.; Wei, S.; Buckner, J.; Jeong, J. C.; Qi, Y.; et al. CHARMM-GUI Input Generator for NAMD, GROMACS, AMBER, OpenMM, and CHARMM/OpenMM Simulations Using the CHARMM36 Additive Force Field. *J. Chem. Theory Comput.* **2016**, *12* (1), 405–413.

(49) Lee, J.; Hitzenberger, M.; Rieger, M.; Kern, N. R.; Zacharias, M.; Im, W. CHARMM-GUI Supports the Amber Force Fields. *J. Chem. Phys.* **2020**, *153* (3), 35103.

(50) Jo, S.; Kim, T.; Iyer, V. G.; Im, W. CHARMM-GUI: A Web-Based Graphical User Interface for CHARMM. *J. Comput. Chem.* **2008**, *29* (11), 1859–1865.

(51) Grant, B. J.; Rodrigues, A. P. C.; ElSawy, K. M.; McCammon, J. A.; Caves, L. S. D. Bio3d: An R Package for the Comparative Analysis of Protein Structures. *Bioinformatics* **2006**, *22* (21), 2695–2696.

(52) Team, Rs.; RStudio Team. RStudio: Integrated Development Environment for R. Boston, MA 2016.

(53) Neuwirth, E. RColorBrewer: ColorBrewer Palettes. 2014.